Neuron
Article

Distinct Roles of Segregated Transmission of the Septo-Habenular Pathway in Anxiety and Fear

Takashi Yamaguchi,[1,2] Teruko Danjo,[1] Ira Pastan,[3] Takatoshi Hikida,[1,4] and Shigetada Nakanishi[1,*]
[1]Department of Systems Biology, Osaka Bioscience Institute, Suita, Osaka 565-0874, Japan
[2]Department of Aging Science, Graduate School of Medicine, Osaka University, Suita, Osaka 565-0871, Japan
[3]Laboratory of Molecular Biology, National Cancer Institute, National Institutes of Health, Bethesda, MD 20892-4264, USA
[4]Present address: Department of Research and Drug Discovery, Medical Innovation Center, Kyoto University Graduate School of Medicine, Sakyo-ku, Kyoto 606-8501, Japan
*Correspondence: snakanis@obi.or.jp
http://dx.doi.org/10.1016/j.neuron.2013.02.035

SUMMARY

The posterior septum consisting of the triangular septum (TS) and the bed nucleus of the anterior commissure (BAC) is predominantly linked with the medial habenula (MHb) and has been implicated in the control of anxiety and fear responses. However, its anatomical and functional linkage has largely remained elusive. We established a transgenic mouse model in which the TS and BAC projection neurons were visualized by GFP fluorescence and selectively eliminated by immunotoxin-mediated cell targeting. The linkage between the TS/BAC and the MHb constitutes two parallel pathways composed of the TS-ventral MHb, the core part of the interpeduncular nucleus (IPN), and the BAC-dorsal MHb, the peripheral part of the IPN. Ablation of the TS and BAC projection neurons selectively impaired anxiety and enhanced fear responses and learning, respectively. Inputs from the TS and BAC to the MHb are thus segregated by two parallel pathways and play specialized roles in controlling emotional behaviors.

INTRODUCTION

In the mammalian brain, the septum and the habenula are tightly interconnected and are thought to be a key linkage between the limbic forebrain and the midbrain (Lecourtier and Kelly, 2007; Risold, 2004; Sutherland, 1982). The septum is divided into the lateral, medial, and posterior septum (LS, MS, and PS, respectively); and the PS is further subdivided into the triangular septum (TS) and the bed nucleus of the anterior commissure (BAC) (Risold, 2004). The habenula also forms a nuclear complex, which is subdivided into the lateral and medial habenula (LHb and MHb, respectively) (Andres et al., 1999). The TS and BAC mostly send efferent projections to the MHb, which in turn predominantly innervates the interpeduncular nucleus (IPN) (Herkenham and Nauta, 1979; Qin and Luo, 2009; Swanson and Cowan, 1979). The IPN mainly projects to the midbrain raphe nuclei (Groenewegen et al., 1986) and the septo-habenular pathway has been implicated in the control of emotional behaviors including anxiety and fear responses (Risold, 2004; Sutherland, 1982; Wilcox et al., 1986). However, both the septum and habenula are organized as an assembly of multiple nuclei, and there was previously no suitable and reliable approach to dissect the anatomical and functional linkages among the TS, BAC, and MHb. The functional roles of these neural linkages in emotional behaviors thus have largely remained elusive.

To address the key linkage of the septo-habenular pathway, we applied the immunotoxin (IT)-mediated cell targeting (IMCT) technique (Watanabe et al., 1998). In this technique, the fusion protein of the human interleukin 2 receptor α subunit (hIL-2R) and GFP was transgenically expressed in a specific neuronal cell type under the control of a neuron-specific promoter (Kaneko et al., 2000; Watanabe et al., 1998; Yoshida et al., 2001). The hIL-2R/GFP-expressing cell type was then killed and eliminated by injection of the IT, which is composed of a monoclonal hIL-2R antibody fused to pseudomonous exotoxin (Watanabe et al., 1998).

The present investigation indicated that the promoter of metabotropic glutamate receptor subtype 2 (mGluR2) directed the specific expression of hIL-2R/GFP in the TS and BAC and distributed it to the MHb. Injection of IT into the TS and BAC then allowed us to selectively eliminate the TS and BAC neurons that innervated the ventral two-thirds of the MHb (vMHb) and the dorsal one-third of the MHb (dMHb), respectively. Here we report that elimination of the TS and BAC projection neurons caused distinct impairment of anxiety-related and fear-directed behaviors, respectively. Neural inputs of the TS and BAC are thus segregated via the parallel TS-vMHb-IPN and BAC-dMHb-IPN pathways and play a specialized role in anxiety- and fear-related emotional behaviors.

RESULTS

Topography of the Septo-Habenular Pathways

In the transgenic mice we used, the integrated transgene consisted of the 5′-upstream genomic sequence containing the first and second exons of the mouse mGluR2 gene and the hIL-2R cDNA fused in frame upstream of the GFP cDNA, then followed by the polyadenylation signal (Watanabe et al., 1998). This promoter faithfully recapitulated the specific expression of the hIL-2R/GFP fusion gene in many mGluR2-expressing neurons with

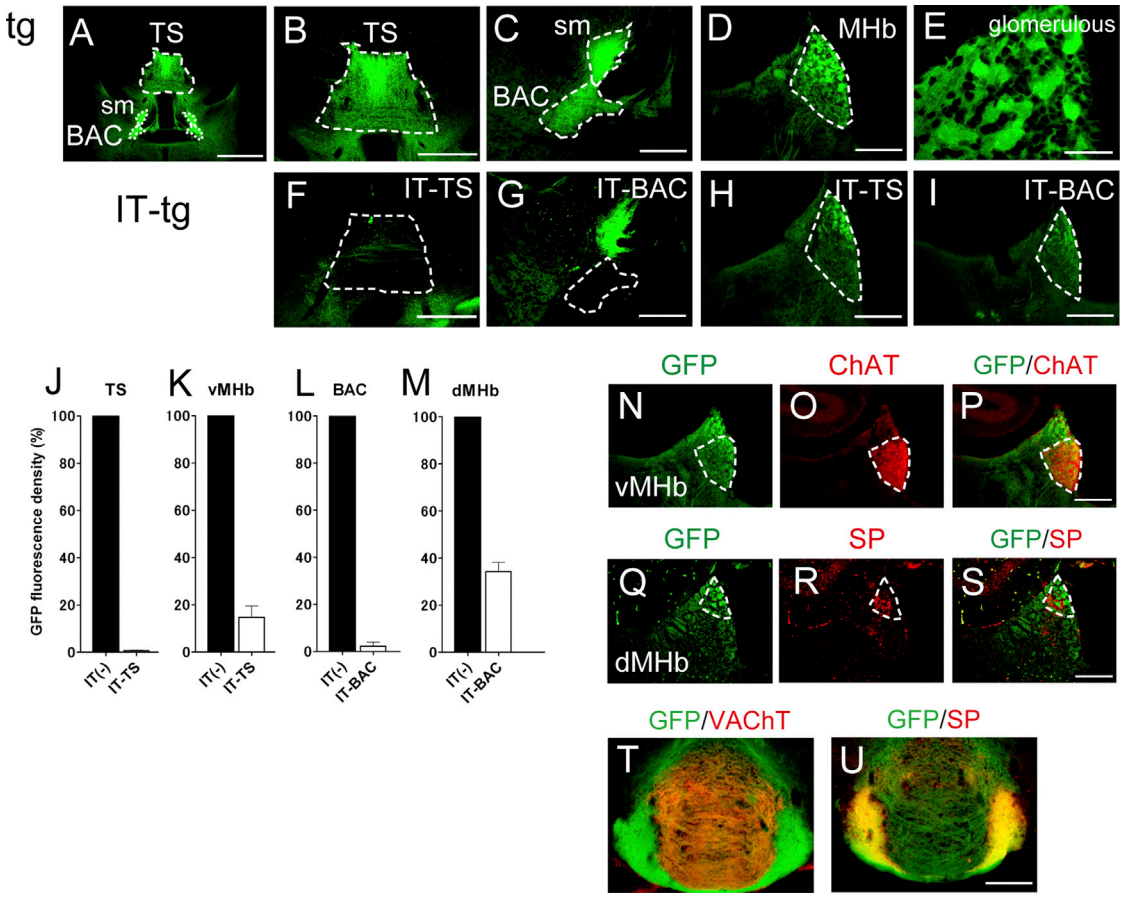

Figure 1. Specific Ablation of Cell Bodies and Their Projections in IT-Injected Transgenic Mice

(A–I) GFP fluorescence in the region covering the TS, BAC, stria medullaris (sm) (A), TS (B), BAC and sm (C), and MHb (D) of IT-uninjected transgenic mice (tg) is shown for comparison with that in the IT-injected TS (F), IT-injected BAC (G), and the MHb after IT injection into the TS (H) and BAC (I) of transgenic mice (IT-tg). Note that the GFP-positive sm in the BAC-ablated mice (G) is derived from GFP-positive TS cells. GFP-positive glomerular structures are shown by magnifying the view of the MHb of the transgenic mouse (E). Scale bars represent 1 mm in (A), 500 μm in (B) and (F), 200 μm in (C), (D), and (G)–(I), and 50 μm in (E).

(J–M) Densities of GFP fluorescence in the TS (J), BAC (L), vMHb (K), and dMHb (M) were measured after IT injection into the TS (J and K) or BAC (L and M) of transgenic mice and compared with those of the corresponding IT-uninjected transgenic mice (n = 5 each). Columns and error bars represent the mean ± SEM, respectively; two-tailed paired Student's t test between IT-injected and uninjected transgenic mice, $p < 0.0001$.

(N–S) A restricted overlap of ChAT immunoreactivity (O and P) and SP hybridization signals (R and S) at the GFP-positive vMHb (N and P) and dMHb (Q and S) of transgenic mice, respectively. Scale bar represents 200 μm.

(T and U) Separate projections of GFP-positive, cholinergic (T) and SPergic neurons (U) of the MHb into the IPN were identified by the VAChT and SP immunoreactivities, respectively. Scale bar represents 200 μm. See also Figures S4 and S5.

some exceptional failure of the transgene expression in particular cell types such as dentate gyrus granule cells (Watanabe et al., 1998). The injection of IT was capable of successfully eliminating a GFP-expressing neuronal cell type from the complex nuclei of the adult brain (Kaneko et al., 2000; Watanabe et al., 1998; Yoshida et al., 2001).

Previous studies indicated that mGluR2 mRNA is expressed in TS neurons and that mGluR2 immunoreactivity is high at the TS and BAC in the posterior septum (Ohishi et al., 1993, 1998). We examined the expression profile of GFP fused to hIL-2R under the control of the mGluR2 promoter in transgenic mice (Watanabe et al., 1998). Extensive GFP fluorescence was detected in cell bodies of the TS and at their axon terminals in characteristic glomerular structures of the MHb (Figures 1A, 1B, 1D, and 1E). The TS has been differently defined by different studies, but Résibois and Rogers (1992) reported that the TS is strongly calretinin immunopositive and is distinguished from the neighboring, weak calretinin-immunoreactive septofimbrial nucleus. Because the GFP fluorescence and carletinin immunoreactivity completely overlapped in transgenic mice (see Figures S5A and S5B available online), the GFP-positive TS was defined by following the references of Résibois and Rogers (1992) and Risold (2004). In addition to the TS, conspicuous GFP fluorescence was observed in cell bodies of the BAC as well as in their projection terminals in the glomerular structures of the MHb (Figures 1A and 1C–1E). Importantly, the GFP fluorescence was not detected in either the MS or the LS (see Figures S1D and S1E) and only sparsely observed in the bed nucleus of the stria

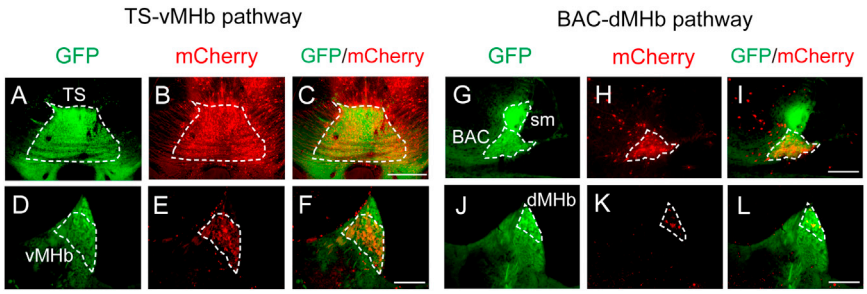

Figure 2. Anterograde Tracing of the TS and BAC into the vMHb and dMHb, Respectively

AAV-CAG-mCherry (red) injected into the TS (A–C) and BAC (G–I) separately labeled the GFP-positive vMHb (D–F) and dMHb (J–L), respectively. Scale bars represent 500 μm in (A)–(C) and 200 μm in (D)–(L). See also Figures S1–S3.

terminalis (BNST) (see Figure S4M). The results thus indicated that the hIL-2R was exclusively expressed in the TS and BAC within the septal nuclei.

The GFP fluorescence of the MHb was distributed in both the vMHb and the dMHb (Figures 1N–1S), and these subregions were identified by immunoreactivity of choline acetyltransferase (ChAT) and in situ hybridization signals of substance P (SP) mRNA, respectively (Contestabile et al., 1987; Quina et al., 2009). Furthermore, the GFP fluorescence was positive at both the central core of the IPN (cIPN) and the peripheral region of the IPN (pIPN) (Figures 1T and 1U), which were clearly distinguished by the vesicular acetylcholine transporter (VAChT)-immunoreactive projection terminals of the cholinergic vMHb neurons and the SP-immunoreactive terminals of the SPergic dMHb neurons, respectively (Quina et al., 2009). Thus, the hIL-2R/GFP fusion protein was not only distributed at the projection terminals of the TS and BAC but also expressed in both vMHb and dMHb neurons.

Because the TS and BAC were clearly bordered by GFP fluorescence in transgenic mice, we examined precise interconnections of the TS, BAC, and MHb by anterograde tracing with AAV-CAG-mCherry and retrograde tracing with cholera toxin-B conjugated to the dye Alexa Fluor 594. The anterogradely labeled axons from the TS and BAC exclusively projected to the vMHb and dMHb, respectively; and no other brain regions were labeled with either tracing (Figures 2A–2L). The predominant projections from the TS/BAC to the MHb were substantiated by retrograde tracing of the MHb, in which both the TS and BAC were strongly labeled by tracer injection into the MHb (Figures 3A–3J). When the TS was retrogradely labeled, prominent projections were detected from the hippocampus and median raphe, and little innervations were noted from either the MS or LS (Figure S1). In retrograde tracing of the BAC, considerable innervations were observed from the medial amygdala and median raphe and moderate innervations from the subiculum; but only a few from the LS and almost none from the TS or MS were noted (Figure S2). Additional retrograde tracing confirmed robust innervations from the LS to the MS, but no connections from the TS or BAC to either the MS or the LS (Figure S3). These analyses indicated that the TS and the BAC predominantly and in a segregated fashion sent their projections to the two MHb subregions, i.e., the vMHb and the dMHb, respectively, without any innervations to other septal nuclei (Figure 3K). The transgenic mice thus allowed us to dissect the afferent-dependent function of the MHb by separate ablation of neuronal cells from the TS and BAC.

Selective Elimination of the TS and BAC Projection Neurons

IT is composed of a monoclonal hIL-2R antibody fused to bacterial toxin and selectively binds to and kills hIL-2R-expressing neuronal cells (Watanabe et al., 1998). IT was bilaterally microinjected in a stereotaxic manner into either the TS or the BAC of adult transgenic mice. When the GFP fluorescence was visualized and its intensity was quantified in the brain sections 2 weeks after IT injection, GFP-positive cells were ablated in both the TS and the BAC by more than 90% (Figures 1F–1M). In both the TS and BAC, the calretinin immunoreactivity also disappeared after the IT injection into the transgenic mice but not into the wild-type (WT) mice (Figures S4A–S4F). Because the GFP fluorescence was intensely but diffusely distributed in the TS and BAC, the selective and efficient elimination of the projection neurons was further confirmed by counting the cell number of calretinin-immunoreactive cells in the IT-injected and uninjected transgenic mice in an unbiased stereological manner (Figures S4G–S4L). The IT injection into either the TS or BAC eliminated more than 80% of calretinin-positive cells of the targeted nuclei in both cases (Figures S4P and S4Q). Furthermore, the IT injection into either the TS or the BAC had no effect on sparsely distributed GFP-positive neurons in the neighboring BNST (Figures S4M–S4O and S4R). When the TS cells were visualized by DAPI staining, the IT injection significantly diminished TS cells (Figures S5A–S5F). However, the IT had no effect on GFP-negative, parvalbumin-immunoreactive interneurons in the TS (Figures S5G–S5J).

The MHb neuronal cells expressed the GFP fusion protein (Figures 1D, 1T, and 1U). It was thus difficult to quantify how effectively the TS- and BAC-originating axon terminals were eliminated in the MHb by IT injection. Despite this underestimating situation, the IT injection into the TS and the BAC markedly decreased the intensity of GFP fluorescence in the vMHb and dMHb by more than 80% and 60%, respectively (Figures 1K and 1M). Collectively, IT selectively and almost completely eliminated both the TS and BAC projection neurons in the transgenic mice.

Effects of Ablation of the TS or BAC Projection Neurons on Animal Behaviors

We addressed whether selective ablation of either the TS or the BAC could alter emotional behaviors by performing several different behavioral tests (Gould, 2009) 2 weeks after IT injection into the respective nuclei of transgenic and WT mice. In the open-field test, the locomotor activity of the TS-ablated mice

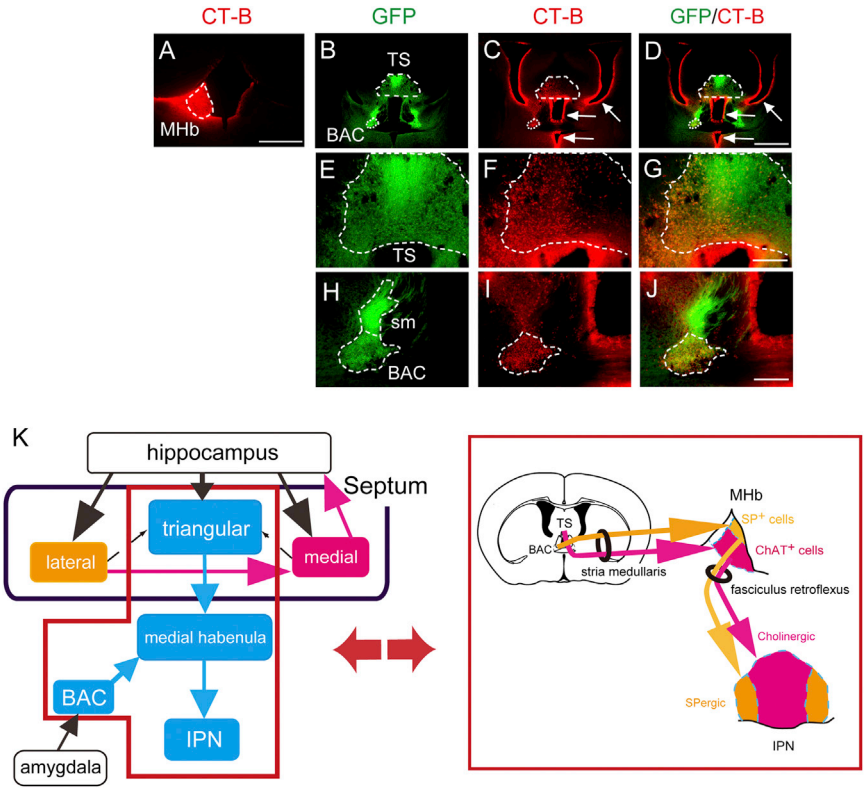

Figure 3. Retrograde Tracing of the MHb into the TS and BAC

(A–J) Unilateral injection of a retrograde tracer (red) into the MHb (A) showed prominent labeling at the ipsilateral side of the GFP-positive TS and BAC of transgenic mice (B–D). Arrows in (C) and (D) indicate false staining of ependymal cells lining the ventricles, which resulted from leakage of a tracer into the ventricles close to the MHb during removal of a tracer-filled syringe from the brain. Magnified views of labeling of the TS and BAC are shown in (E)–(G) and (H)–(J), respectively. Scale bars represent 500 μm in (A), 1 mm in (B)–(D), and 200 μm in (E)–(J).

(K) Schematic drawing focusing on the TS-vMHb-cIPN and the BAC-dMHb-pIPN pathways. Left: solid arrows, predominant projections; dashed arrows, rare projections. See also Figures S1–S3.

was significantly reduced as compared with that of the WT mice (TS-ablated, 8,782 ± 685 cm/hr; IT-WT, 12,560 ± 973 cm/hr, $p < 0.01$; Figure 4A). Despite this decrease in locomotor activity, the TS-ablated and WT mice comparably stayed in the central part of the open field (TS-ablated, 1,415 ± 92 cm/hr; IT-WT, 1,425 ± 189 cm/hr). Consequently, traveling activity in the central field relative to total locomotor activity was significantly higher in the TS-ablated mice than in the WT ones (TS-ablated, 16.4% ± 0.78%; IT-WT, 11.4% ± 1.3%, $p < 0.01$; Figure 4A). This finding suggested that the anxiety-related behavior was reduced by ablation of the TS.

The deficit in anxiety-related response in the TS-ablated mice was further examined by performing elevated plus maze and marble-burying analyses. In the elevated plus maze test, the IT-WT mice were scared of visiting an open arm of the elevated maze and avoided entering it from a central space. In contrast, the TS-ablated mice showed a significant increase in both the frequency to enter the open arm and time staying in it (for frequency, TS-ablated, 23.8% ± 4.5%; IT-WT, 9.4% ± 3.7%, $p < 0.05$; for staying time, TS-ablated, 20.7% ± 4.5%; IT-WT, 4.8% ± 2.0%, $p < 0.01$; Figures 4B and 4D). In the marble-burying test, mice were nervous about glossy glass marbles placed over the bedding material and tried to bury the marbles under a layer of the material. In this test, the TS-ablated mice showed a significant reduction in the number of marbles buried compared with the IT-WT mice (TS-ablated, 9.5 ± 2.0; IT-WT, 16.2 ± 1.0, $p < 0.01$; Figures 4C and 4E). Thus, all three of the above behavioral tests demonstrated that ablation of the TS impaired anxiety-related behavior.

In contrast to the TS-ablated mice, the BAC-ablated mice showed no such deficits in anxiety-related behaviors, when they were analyzed by the open-field test (for total mobility, BAC-ablated, 12,400 ± 873 cm/hr; IT-WT, 12,850 ± 787 cm/hr, $p = 0.71$; for center traveled, BAC-ablated, 14.6% ± 0.70%; IT-WT, 13.8% ± 0.74%, $p = 0.41$; Figure 4F), the elevated plus maze test (for frequency of open-arm entry, BAC-ablated, 17.0% ± 4.2%; IT-WT, 19.3% ± 2.9%, $p = 0.66$; for staying time, BAC-ablated, 6.3% ± 2.1%; IT-WT, 8.4% ± 1.4%, $p = 0.45$; Figure 4G), and the marble-burying test (BAC-ablated, 15.4 ± 1.5; IT-WT, 16.6 ± 1.6, $p = 0.62$; Figure 4H). Thus, ablation of the TS, but not that of the BAC, severely impaired anxiety-related behavior.

The genetical disruption of the zebrafish dorsal habenula corresponding to the mammalian MHb has been reported to enhance experience-dependent fear responses to electrical shocks (Agetsuma et al., 2010; Lee et al., 2010). We examined fear-directed responses in the TS- and BAC-ablated mice. When freezing responses were measured immediately after presentation of electric shocks, the TS-ablated mice showed gradually increasing postshock freezing comparable to that of the WT mice (TS-ablated versus IT-WT, effects of shock/freezing on genotype, $F_{1,75} = 0.46$, $p = 0.51$; time, $F_{5,75} = 83.8$, $p < 0.0001$; interaction genotype × time, $F_{5,75} = 0.59$, $p = 0.71$; Figure 5A). In contrast, the BAC-ablated mice froze more severely after footshocks than the WT mice did (BAC-ablated versus IT-WT, effects of shock/freezing on genotype, $F_{1,75} = 13.2$, $p < 0.01$; time, $F_{5,75} = 83.9$, $p < 0.0001$; interaction genotype × time, $F_{5,75} = 4.82$, $p < 0.001$; Figure 5A).

Then, passive avoidance learning was tested by performing a one-trial inhibitory avoidance task (Hikida et al., 2010). In this task, mice received electric footshocks when they entered from a lighted chamber to a preferred dark chamber. Fear memory was then tested 24 hr later by measuring latencies in which the mice avoided entering the electrically shocked chamber. The TS-ablated mice and the WT mice comparably avoided

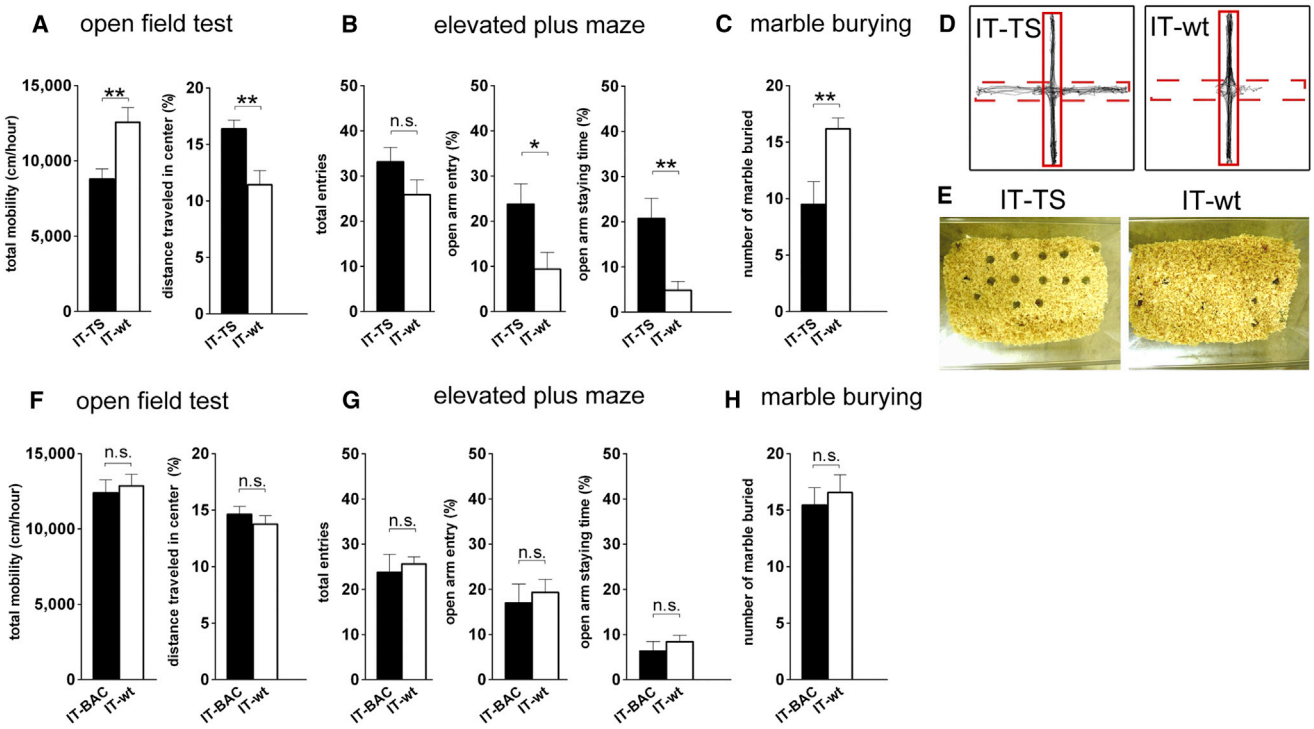

Figure 4. Impairments of Anxiety-Related Behaviors of the TS-Ablated Mice, but Not of Those of the BAC-Ablated Mice

(A and F) Total mobility and percentages of the distance traveled in the central square were measured for the TS-ablated (n = 9; A), BAC-ablated (n = 10; F), and IT-injected WT (n = 8; A or n = 9; F) mice in the open-field test.

(B and G) In the elevated plus maze test, the total number of entries from a central square to the open and closed arms, percentages of entering an open arm, and time staying in the open arm were measured for the TS-ablated (n = 10; B) and BAC-ablated (n = 9; G) mice and compared with those for the IT-injected WT mice (n = 10; B or n = 8; G).

(C and H) The number of buried marbles was measured for the TS-ablated (n = 10; C), BAC-ablated (n = 9; H), and IT-injected WT (n = 12; C or n = 9; H) mice. Columns and bars represent the mean ± SEM, respectively. Statistical analysis between IT-injected transgenic and WT mice was conducted by the unpaired two-tailed Student's t test. *$p < 0.05$, **$p < 0.01$, n.s., not significant.

(D and E) Typical examples of trajectories in the elevated plus maze test (D) and marble-burying test (E) are shown. In the elevated plus maze, dashed and solid lines indicate open and closed arms, respectively.

entering the dark chamber 24 hr after electric footshocks (after conditioning, TS-ablated, 68.9 ± 31.2 s; IT-WT, 59.1 ± 12.9 s, $p = 0.77$; Figure 5B). Importantly, the BAC-ablated mice more sensitively avoided entering the shocked chamber (after conditioning, BAC-ablated 141.7 ± 31.5 s; IT-WT, 59.3 ± 22.6 s, $p < 0.05$; Figure 5B). Thus, in contrast to anxiety-related behavior, ablation of the BAC, but not the TS, severely changed fear responses and fear learning. Therefore, the segregated input transmission of the TS-vMHb and the BAC-dMHb plays a distinct role in controlling the anxiety-related and fear-directed behaviors, respectively.

DISCUSSION

This investigation established a transgenic mouse model in which the GFP/hIL-2R fusion protein was specifically expressed in the TS and BAC within the septal nuclei. In combination with anterograde and retrograde tracings, this model allowed us to precisely characterize a distinct linkage between the TS/BAC and the MHb, which constitutes two parallel pathways composed of the TS-vMHb-cIPN and the BAC-dMHb-pIPN pathways. Previous lesion and pharmacological studies have implicated the septo-habenular pathway in anxiety- or fear-related behaviors (Menard and Treit, 1996; Murphy et al., 1996; Sutherland, 1982; Thornton and Bradbury, 1989; Wilcox et al., 1986). However, these analyses limited the precise characterization of individual nuclei in the complex nuclear organizations of both the septum and habenula in emotional behaviors. This investigation thus aimed at exploring how the two parallel septo-habenular pathways could regulate anxiety-related and fear responses. The present investigation explicitly demonstrated that the segregated inputs from the TS and BAC to the vMHb and dMHb, respectively, play specialized roles in controlling anxiety-related and fear-directed behaviors.

Recently, the function of the dorsal habenula (dHb) of zebrafish, which corresponds to the mammalian MHb, was investigated by genetic manipulation and photobleaching techniques (Agetsuma et al., 2010; Jesuthasan, 2012; Lee et al., 2010; Okamoto et al., 2012). These studies indicated that blockade of neural transmission in the zebrafish dHb extensively enhanced experience-dependent fear responses (Agetsuma et al., 2010; Lee et al., 2010). The zebrafish dHb is subdivided into two

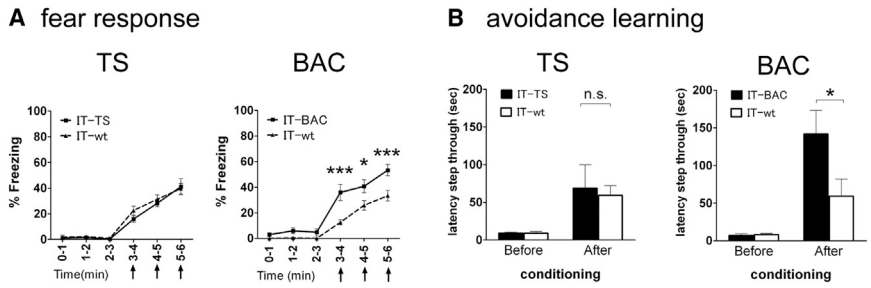

Figure 5. Impairments of Fear-Directed Behaviors of the BAC-Ablated Mice, but Not Those of the TS-Ablated Ones

(A) Percentages of freezing were determined for a 1 min period after giving electric shocks at 3, 4, and 5 min (arrows). Marks and bars represent the mean ± SEM, respectively; TS-ablated (n = 9), BAC-ablated (n = 9), and IT-injected WT (n = 8) mice. Two-way ANOVA was conducted between time point and genotype, followed by Bonferroni post hoc test; *p < 0.05, ***p < 0.001.

(B) Avoidance learning was tested by use of the one-trial inhibitory avoidance task performed by the TS-ablated (n = 9), BAC-ablated (n = 7), and IT-injected WT (n = 9 or 10) mice. Columns and bars represent the mean ± SEM, respectively. Statistical analysis between IT-injected transgenic and WT mice was conducted by two-way ANOVA followed by Bonferroni post hoc test. *p < 0.05, n.s., not significant.

subdomains, which are termed as lateral and medial parts of the dHb according to their separate organization (dHb_L and dHb_M, respectively) (Aizawa et al., 2005; Amo et al., 2010). In mutational analysis, the mammalian *Narp* (*neuronal activity regulated pentraxin*) gene homolog was used to direct the expression of the transmission-blocking tetanus toxin (TN) in a subdomain of the zebrafish dHb (Agetsuma et al., 2010). In mammals, the *Narp* gene is mainly expressed in the SP-positive dMHb (Reti et al., 2002); and consistent with this expression profile, the TN was specifically expressed in the dHb_L, but not in the dHb_M, of zebrafish (Agetsuma et al., 2010). Thus, the dHb_L of zebrafish most likely corresponds to the dMHb of mammals. Importantly, similar to blockade of the BAC-dMHb pathway in transgenic mice, the TN-mediated silencing restricted to the zebrafish dHb_L enhanced experience-dependent fear responses (Agetsuma et al., 2010). Therefore, the organization and the functional specificity of the MHb are evolutionally conserved between zebrafish and mice, and such conservation implies that the segregated input transmission in the septo-habenular pathway plays an important role in controlling fear-directed behavior.

Previous studies reported that disruption of either the MS or LS impaired anxiety-related behavior (Menard and Treit, 1996; Pesold and Treit, 1992; Shin et al., 2009). Because the TS was found to be critical for eliciting anxiety in this study, lesion analysis restricted to the MS was carefully repeated by use of kainic acid treatments; and the data confirmed that the restricted MS lesion also impaired an anxiety-related behavior. In the septal nuclear complex, the TS receives predominant projections from the hippocampus and median raphe but, different from the MS and LS, exclusively projects to the vMHb with no obvious interconnections with either the MS or the LS. The TS per se thus serves as a distinct, key neural substrate that controls anxiety-related behavior. Noteworthy here is that the TS is not involved in controlling fear response and fear learning. Interestingly, the major afferents, as revealed by retrograde tracings, are different between the TS and the BAC, the former and the latter being the hippocampal dentate gyrus and the medial amygdala, respectively. Furthermore, in relation to the anxiolytic effect of nicotine, the cholinergic cellular components (ChAT and VAChT) are exclusively enriched in the TS-vMHb-cIPN pathway. Accumulated evidence by psychophysiological and gene-targeting studies has pointed out that fear and anxiety are distinguishable as different entities of emotional function (Refojo et al., 2011; Sylvers et al., 2011; Weisstaub et al., 2006). Furthermore, both fear and anxiety are compound behavioral phenotypes controlled by processing of neural information in the integrative neural circuits based on specified innate programs in response to external information inputs (Jesuthasan, 2012; McNaughton and Corr, 2004; Okamoto et al., 2012). The integrative processes that regulate anxiety and fear responses have important psychiatric implications for emotional disorders such as posttraumatic stress disorder, obsessive-compulsive disorder, and depression (Damsa et al., 2009; Gross and Hen, 2004; LeDoux, 2000; Ressler and Mayberg, 2007). Our finding of the segregated parallel pathways in the septo-habenular linkage will help in exploring the diverse information processings involved in anxiety- and fear-directed behaviors and emotional disorders.

EXPERIMENTAL PROCEDURES

Animals and IT Treatment

All animal handling procedures were performed according to the guidelines of Osaka Bioscience Institute. The Ig17 line of heterozygous transgenic mice (Watanabe et al., 1998) and their WT littermates were used for all ablation experiments, and both homozygous and heterozygous transgenic mice were used in tracer experiments. Ten nanograms of IT were dissolved in 1 μl PBS with 1% BSA. After deep anesthesia with 0.9% ketamine and 0.1% xylazine, 1 μl and 0.5 μl of the IT solution were bilaterally injected at three sites/side of the TS and four sites/side of the BAC, respectively, according to the atlas of Franklin and Paxinos (2008). The stereotaxic coordinates of injection into the TS were 0.1, 0.2, or 0.3 mm posterior to the bregma, 0.1 mm lateral to the midline, and 2.25 or 2.75 mm depth from the dura; and those for the BAC were 0.1 or 0.2 mm posterior to the bregma, 0.4 or 0.5 mm lateral to the midline, and 3.6 mm depth from the dura. After behavioral analysis, ablation of targeted neuronal cells by IT injection was confirmed by direct visualization of GFP fluorescence in serially dissected slice preparations. The density of GFP fluorescence was measured by image analysis with software WinROOF V6.1 (Mitani Corporation). In the case of partial cell ablation (more than 30% of the GFP fluorescence remaining) or cell ablation at one side of the targeted nuclei, these data were discarded.

Immunohistochemistry and Cell Counting

Two weeks after IT injection into the TS or BAC, the animals were deeply anesthetized with diethylether and transcardially perfused with PBS, followed by 4% paraformaldehyde in 0.1 M sodium phosphate buffer (PB). Their brains were then removed, postfixed with the same fixative at 4°C overnight, and cryoprotected with 30% sucrose in PB. Coronal sections (50 μm) were prepared and immunostained with the primary antibody. The primary antibodies used were obtained from the following sources: goat polyclonal choline acetyltransferase (ChAT) antibody, rat monoclonal substance P antibody, rabbit polyclonal calretinin antibody, and mouse monoclonal parvalbumin antibody

from Millipore and goat polyclonal vesicular acetylcholine transporter (VAChT) antibody from Santa Cruz. Signals were visualized with the secondary antibody conjugated to Alexa Fluor (Invitrogen). After immunostaining, the sections were mounted with Vectashield containing DAPI (Vector Laboratories) and analyzed under a Zeiss Axioplan 2 microscope or a BZ-9000 digital fluorescence microscope (Keyence). For cell counting, IT was injected or uninjected into either the TS or the BAC of transgenic mice. Two weeks after IT injection, the brain was serially dissected (50 μm thick each) and each of more than 20 contiguous sections covering the TS, BAC, and BNST was immunostained with the calretinin antibody. The number of calretinin-immunoreactive cell bodies of the TS and BAC and that of GFP-positive cells of the BNST were counted in IT-injected and uninjected transgenic mice.

Double Staining with Immunohistochemistry and In Situ Hybridization

Coronal sections (10 μm) were prepared as described above and immunostained with a rabbit polyclonal GFP antibody (Invitrogen), followed by the secondary antibody. The immunostained sections were then hybridized with a DIG-labeled antisense SP riboprobe (residues from +95 to +995, NCBI accession number NM_009311) at 68°C for 12 hr (Watakabe et al., 2007). After having been washed with saline/sodium citrate buffer, the sections were incubated with anti DIG-POD sheep Fab fragment (Roche) and visualized by use of the Tyramide Signal Amplification System (PerkinElmer).

Anterograde and Retrograde Tracings

For anterograde labeling, AAV-CAG-mCherry (1 μl) was unilaterally injected into the TS or the BAC of the Ig17 transgenic mice by the stereotaxic technique: for TS, 0.1 mm posterior to the bregma, the midline, and 2.75 mm depth from the dura; for BAC, 0.1 mm posterior to the bregma, 0.4 mm lateral to the midline, and 3.6 mm depth from the dura. Two weeks after the injection, coronal sections (50 μm) were prepared and analyzed under a Zeiss Axioplan 2 microscope. For retrograde labeling, cholera toxin-B conjugated to Alexa Fluor 594 (Invitrogen) was unilaterally injected into the following brain regions by the stereotaxic technique, except for bilateral injection into the LS: for MHb, 2.0 mm posterior to the bregma, 0.25 mm lateral to the midline, and 2.0 mm depth from the dura; for MS, 1.0 mm anterior to the bregma, the midline, and 3.5 mm depth from the dura; for LS, 0.5 mm anterior to the bregma, 0.5 mm lateral to the midline, and 2.5 mm depth from the dura. The coordinates for TS and BAC were the same as those described for anterograde labeling analysis. Ten days after the injection, coronal sections (50 μm) were prepared and analyzed as described above.

Behavioral Analyses

All behavioral experiments were conducted 2 weeks after the IT injection. The open-field test was performed in an open arena (27 × 27 cm) concealed by 20-cm-high walls. The mice were placed in the center of the field, and locomotor activity was measured with an infrared monitor (MED-Associates) for 60 min. The field was divided into five squares, and the distances traveled in the whole field and in the central square were calculated.

The elevated plus maze consisted of a central square (5 × 5 cm), two open arms (25 × 5 cm), and two closed arms (25 × 5 cm) placed 70 cm above the ground. The closed arms were concealed by 20-cm-high walls. Mice were placed in the central square and allowed to explore the maze for 10 min.

In the marble-burying test, 24 glossy glass marbles (10 mm diameter) were placed on sawdust bedding material (5 cm depth; Charles River) in a transparent cage (24 × 45 × 21 cm). Mice were placed in the cage, and the number of marbles buried under the bedding material for 30 min was counted.

Fear responses were analyzed by scoring the number of positive freezing responses divided by the total number of samples at 2 s intervals in a 1 min time period (Hikida et al., 2010). Avoidance behavior was tested by the one-trial inhibitory avoidance task (Hikida et al., 2010). Briefly, when mice moved from a light chamber to a preferred dark chamber in the step-through inhibitory avoidance apparatus, electric shocks were delivered. Fear memory retention was tested 24 hr later by measuring latencies for the mice to enter the electrically shocked dark chamber. All tests of animal behaviors were conducted in a blind manner.

Statistical Analysis

Statistical analysis was conducted by using GraphPad prism 5 (GraphPad Software). Data were analyzed by paired or unpaired t test and one-way or two-way repeated-measures ANOVA.

SUPPLEMENTAL INFORMATION

Supplemental Information includes five figures and can be found with this article online at http://dx.doi.org/10.1016/j.neuron.2013.02.035.

ACKNOWLEDGMENTS

We thank S. Chaki and T. Shimazaki for technical advice on the behavioral analysis. This work was supported by Research Grants-in-Aid 22220005 (S.N.), 23120011 (T.H. and S.N.), and 23680034 (T.H.) from the Ministry of Education, Culture, Sports, Science and Technology of Japan, and by grants from the JST PRESTO Program (T.H.), the Takeda Science Foundation (S.N.), and the Naito Foundation (T.H.).

Accepted: February 4, 2013
Published: April 18, 2013

REFERENCES

Agetsuma, M., Aizawa, H., Aoki, T., Nakayama, R., Takahoko, M., Goto, M., Sassa, T., Amo, R., Shiraki, T., Kawakami, K., et al. (2010). The habenula is crucial for experience-dependent modification of fear responses in zebrafish. Nat. Neurosci. *13*, 1354–1356.

Aizawa, H., Bianco, I.H., Hamaoka, T., Miyashita, T., Uemura, O., Concha, M.L., Russell, C., Wilson, S.W., and Okamoto, H. (2005). Laterotopic representation of left-right information onto the dorso-ventral axis of a zebrafish midbrain target nucleus. Curr. Biol. *15*, 238–243.

Amo, R., Aizawa, H., Takahoko, M., Kobayashi, M., Takahashi, R., Aoki, T., and Okamoto, H. (2010). Identification of the zebrafish ventral habenula as a homolog of the mammalian lateral habenula. J. Neurosci. *30*, 1566–1574.

Andres, K.H., von Düring, M., and Veh, R.W. (1999). Subnuclear organization of the rat habenular complexes. J. Comp. Neurol. *407*, 130–150.

Contestabile, A., Villani, L., Fasolo, A., Franzoni, M.F., Gribaudo, L., Oktedalen, O., and Fonnum, F. (1987). Topography of cholinergic and substance P pathways in the habenulo-interpeduncular system of the rat. An immunocytochemical and microchemical approach. Neuroscience *21*, 253–270.

Damsa, C., Kosel, M., and Moussally, J. (2009). Current status of brain imaging in anxiety disorders. Curr. Opin. Psychiatry *22*, 96–110.

Franklin, K., and Paxinos, G. (2008). The Mouse Brain in Stereotaxic Coordinates, Third Edition (San Diego: Academic Press).

Gould, T.D. (2009). Mood and Anxiety Related Phenotypes in Mice: Characterization Using Behavioral Tests, Springer Protocols, Neuromethods 42 (New York: Humana Press).

Groenewegen, H.J., Ahlenius, S., Haber, S.N., Kowall, N.W., and Nauta, W.J. (1986). Cytoarchitecture, fiber connections, and some histochemical aspects of the interpeduncular nucleus in the rat. J. Comp. Neurol. *249*, 65–102.

Gross, C., and Hen, R. (2004). The developmental origins of anxiety. Nat. Rev. Neurosci. *5*, 545–552.

Herkenham, M., and Nauta, W.J. (1979). Efferent connections of the habenular nuclei in the rat. J. Comp. Neurol. *187*, 19–47.

Hikida, T., Kimura, K., Wada, N., Funabiki, K., and Nakanishi, S. (2010). Distinct roles of synaptic transmission in direct and indirect striatal pathways to reward and aversive behavior. Neuron *66*, 896–907.

Jesuthasan, S. (2012). Fear, anxiety, and control in the zebrafish. Dev. Neurobiol. *72*, 395–403.

Kaneko, S., Hikida, T., Watanabe, D., Ichinose, H., Nagatsu, T., Kreitman, R.J., Pastan, I., and Nakanishi, S. (2000). Synaptic integration mediated by striatal cholinergic interneurons in basal ganglia function. Science *289*, 633–637.

Lecourtier, L., and Kelly, P.H. (2007). A conductor hidden in the orchestra? Role of the habenular complex in monoamine transmission and cognition. Neurosci. Biobehav. Rev. *31*, 658–672.

LeDoux, J.E. (2000). Emotion circuits in the brain. Annu. Rev. Neurosci. *23*, 155–184.

Lee, A., Mathuru, A.S., Teh, C., Kibat, C., Korzh, V., Penney, T.B., and Jesuthasan, S. (2010). The habenula prevents helpless behavior in larval zebrafish. Curr. Biol. *20*, 2211–2216.

McNaughton, N., and Corr, P.J. (2004). A two-dimensional neuropsychology of defense: fear/anxiety and defensive distance. Neurosci. Biobehav. Rev. *28*, 285–305.

Menard, J., and Treit, D. (1996). Lateral and medial septal lesions reduce anxiety in the plus-maze and probe-burying tests. Physiol. Behav. *60*, 845–853.

Murphy, C.A., DiCamillo, A.M., Haun, F., and Murray, M. (1996). Lesion of the habenular efferent pathway produces anxiety and locomotor hyperactivity in rats: a comparison of the effects of neonatal and adult lesions. Behav. Brain Res. *81*, 43–52.

Ohishi, H., Shigemoto, R., Nakanishi, S., and Mizuno, N. (1993). Distribution of the messenger RNA for a metabotropic glutamate receptor, mGluR2, in the central nervous system of the rat. Neuroscience *53*, 1009–1018.

Ohishi, H., Neki, A., and Mizuno, N. (1998). Distribution of a metabotropic glutamate receptor, mGluR2, in the central nervous system of the rat and mouse: an immunohistochemical study with a monoclonal antibody. Neurosci. Res. *30*, 65–82.

Okamoto, H., Agetsuma, M., and Aizawa, H. (2012). Genetic dissection of the zebrafish habenula, a possible switching board for selection of behavioral strategy to cope with fear and anxiety. Dev. Neurobiol. *72*, 386–394.

Pesold, C., and Treit, D. (1992). Excitotoxic lesions of the septum produce anxiolytic effects in the elevated plus-maze and the shock-probe burying tests. Physiol. Behav. *52*, 37–47.

Qin, C., and Luo, M. (2009). Neurochemical phenotypes of the afferent and efferent projections of the mouse medial habenula. Neuroscience *161*, 827–837.

Quina, L.A., Wang, S., Ng, L., and Turner, E.E. (2009). Brn3a and Nurr1 mediate a gene regulatory pathway for habenula development. J. Neurosci. *29*, 14309–14322.

Refojo, D., Schweizer, M., Kuehne, C., Ehrenberg, S., Thoeringer, C., Vogl, A.M., Dedic, N., Schumacher, M., von Wolff, G., Avrabos, C., et al. (2011). Glutamatergic and dopaminergic neurons mediate anxiogenic and anxiolytic effects of CRHR1. Science *333*, 1903–1907.

Résibois, A., and Rogers, J.H. (1992). Calretinin in rat brain: an immunohistochemical study. Neuroscience *46*, 101–134.

Ressler, K.J., and Mayberg, H.S. (2007). Targeting abnormal neural circuits in mood and anxiety disorders: from the laboratory to the clinic. Nat. Neurosci. *10*, 1116–1124.

Reti, I.M., Reddy, R., Worley, P.F., and Baraban, J.M. (2002). Prominent Narp expression in projection pathways and terminal fields. J. Neurochem. *82*, 935–944.

Risold, P.Y. (2004). The septal region. In The Rat Nervous System, G. Paxinos, ed. (San Diego, CA: Academic Press), pp. 605–632.

Shin, J., Gireesh, G., Kim, S.W., Kim, D.S., Lee, S., Kim, Y.S., Watanabe, M., and Shin, H.S. (2009). Phospholipase C β 4 in the medial septum controls cholinergic theta oscillations and anxiety behaviors. J. Neurosci. *29*, 15375–15385.

Sutherland, R.J. (1982). The dorsal diencephalic conduction system: a review of the anatomy and functions of the habenular complex. Neurosci. Biobehav. Rev. *6*, 1–13.

Swanson, L.W., and Cowan, W.M. (1979). The connections of the septal region in the rat. J. Comp. Neurol. *186*, 621–655.

Sylvers, P., Lilienfeld, S.O., and LaPrairie, J.L. (2011). Differences between trait fear and trait anxiety: implications for psychopathology. Clin. Psychol. Rev. *31*, 122–137.

Thornton, E.W., and Bradbury, G.E. (1989). Effort and stress influence the effect of lesion of the habenula complex in one-way active avoidance learning. Physiol. Behav. *45*, 929–935.

Watakabe, A., Ichinohe, N., Ohsawa, S., Hashikawa, T., Komatsu, Y., Rockland, K.S., and Yamamori, T. (2007). Comparative analysis of layer-specific genes in Mammalian neocortex. Cereb. Cortex *17*, 1918–1933.

Watanabe, D., Inokawa, H., Hashimoto, K., Suzuki, N., Kano, M., Shigemoto, R., Hirano, T., Toyama, K., Kaneko, S., Yokoi, M., et al. (1998). Ablation of cerebellar Golgi cells disrupts synaptic integration involving GABA inhibition and NMDA receptor activation in motor coordination. Cell *95*, 17–27.

Weisstaub, N.V., Zhou, M., Lira, A., Lambe, E., González-Maeso, J., Hornung, J.P., Sibille, E., Underwood, M., Itohara, S., Dauer, W.T., et al. (2006). Cortical 5-HT2A receptor signaling modulates anxiety-like behaviors in mice. Science *313*, 536–540.

Wilcox, K.S., Christoph, G.R., Double, B.A., and Leonzio, R.J. (1986). Kainate and electrolytic lesions of the lateral habenula: effect on avoidance responses. Physiol. Behav. *36*, 413–417.

Yoshida, K., Watanabe, D., Ishikane, H., Tachibana, M., Pastan, I., and Nakanishi, S. (2001). A key role of starburst amacrine cells in originating retinal directional selectivity and optokinetic eye movement. Neuron *30*, 771–780.

Neuron, Volume *78*

Supplemental Information

Distinct Roles of Segregated Transmission of the Septo-Habenular Pathway in Anxiety and Fear

Takashi Yamaguchi, Teruko Danjo, Ira Pastan, Takatoshi Hikida, and Shigetada Nakanishi

Supplemental Figures

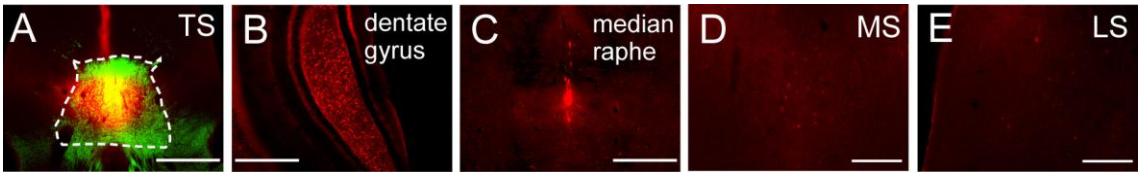

Figure S1, related to Figures 2 and 3. Retrograde Labeling Analysis of the TS Projections.

The brain was serially dissected 10 days after injection of cholera toxin-B conjugated to the dye Alexa Fluor 594 (red) into the TS of transgenic mice (A). Prominent labeling was detected in the hippocampal dentate gyrus (B) and the median raphe (C). Only a few cells were sparsely labeled in the MS (D) and LS (E). Scale bars, 500 µm (A-C); 200 µm (D and E).

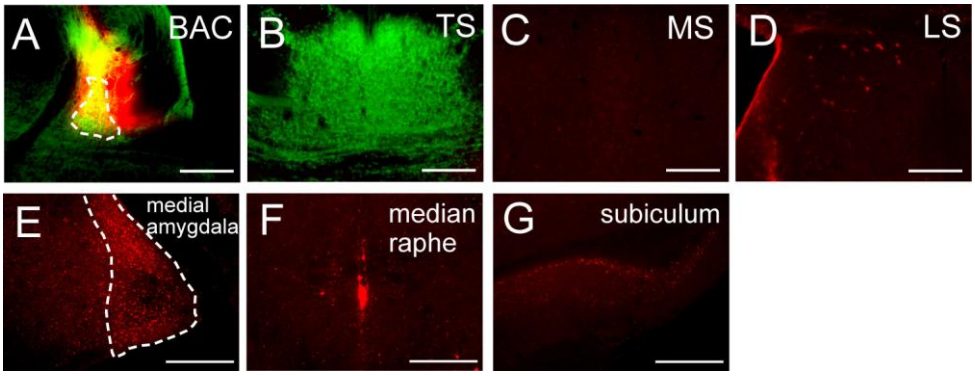

Figure S2, related to Figures 2 and 3. Retrograde Labeling Analysis of the BAC Projections.

The brain was serially dissected 10 days after injection of cholera toxin-B conjugated to the dye Alexa Fluor 594 (red) into the BAC (A). No labeling was observed in the TS (B) or the MS (C). Cells labeled in the LS (D) were sparse. Prominent labeling was detected in the medial amygdala (E) and the median raphe (F), with moderate labeling observed in the subiculum (G). Scale bars, 200 μm (A-D); 500 μm (E-G).

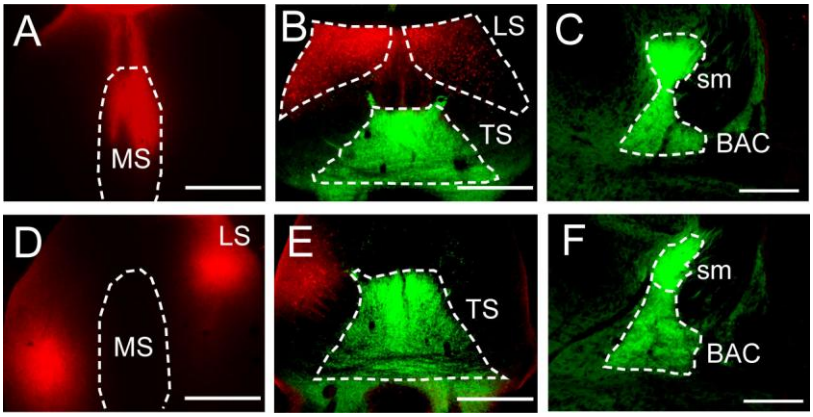

Figure S3, related to Figures 2 and 3. Retrograde Labeling Analysis of the MS and LS Projections.

The brain was serially dissected 10 days after injection of cholera toxin-B conjugated to the dye Alexa Fluor 594 (red) into either the MS (A) or the LS (D). Injection into the MS prominently labeled the LS (B) but not the TS (B) or BAC (C). Injection into the LS failed to label either the MS (D), TS (E) or BAC (F). Scale bars, 500 µm (A, B, D, and E); 200 µm (C and F).

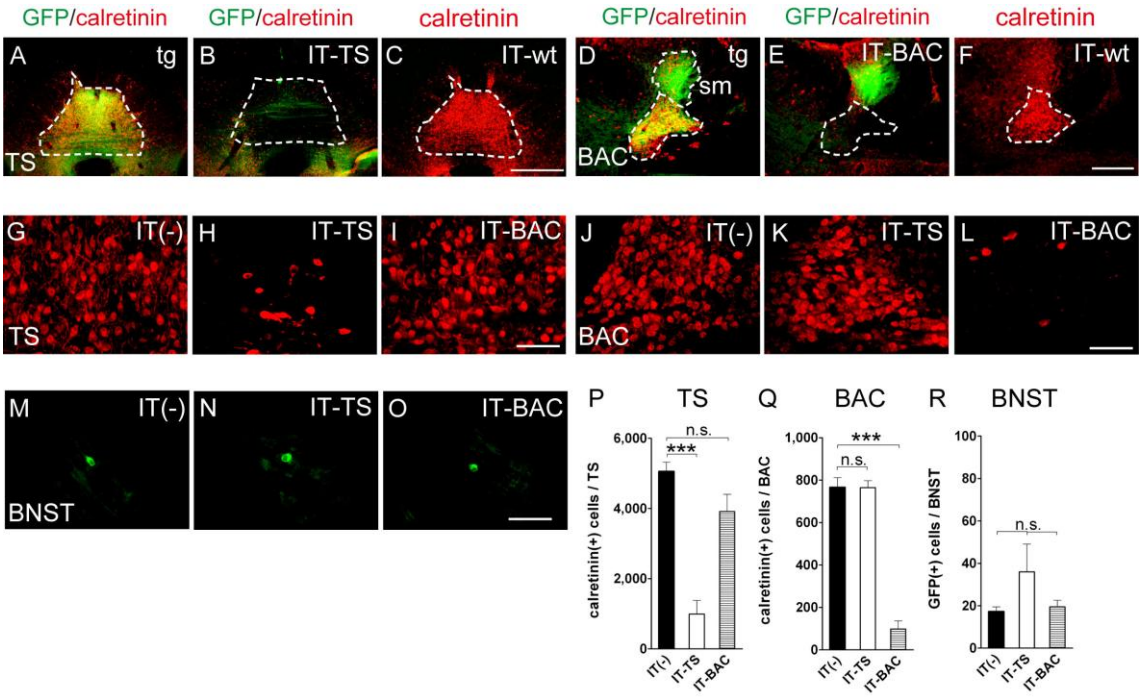

Figure S4, related to Figure 1. Selective Elimination of Projection Neurons of the TS and BAC but not Those of the BNST by IT Treatment.

In (A)-(F), the TS (A-C) or the BAC (D-F) of the transgenic and wt mice was injected or not with IT. The brain was serially dissected (50 μm thick for each section) 2 weeks after the IT injection. The TS and BAC in IT-uninjected (A and D), IT-injected transgenic (B and E), and IT-injected wt mice (C and F) were immunostained with calretinin antibody. The calretinin immunoreactivity (red) almost completely disappeared in both the TS and BAC of the IT-injected transgenic mice. In (G)-(O), IT was injected into the TS (H, K, N) or the BAC (I, L, O) or not injected (G, J, M) in the transgenic mice. The brain was serially dissected (50 μm thick for each section) 2 weeks after the IT injection. The cell bodies of the TS (G-I) and the BAC (J-L) were visualized by calretinin immunostaining, whereas the GFP-positive cell bodies of the BNST (M-O) were detected by GFP fluorescence. The cell number of the respective neurons in the TS (P), BAC (Q), and BNST (R) was counted in each section and summed in a stereological manner (n = 4 animals each). Scale bars, 500 μm (A-C);

200 µm (D-F); 50 µm (G-O). Columns and bars represent the mean ± SEM, respectively. Statistical analysis was conducted by ANOVA followed by Tukey post-hoc test. ***p < 0.001, n.s., not significant.

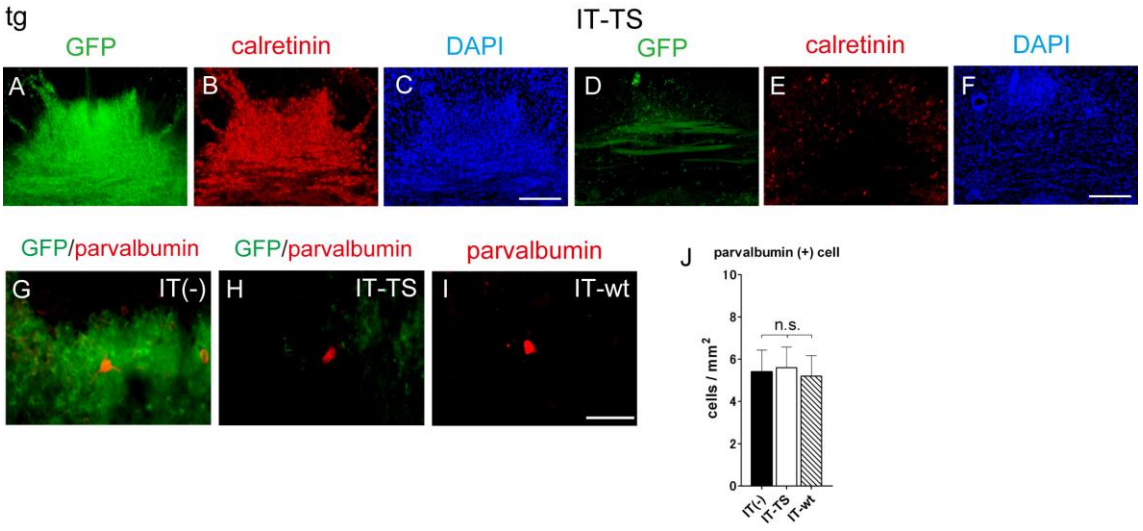

Figure S5, related to Figure 1. Selective Elimination of the GFP-positive TS Neurons by IT treatment.

In (A)-(F), the TS of the transgenic mice was injected (D-F) or not (A-C) with IT. Two weeks after the IT injection, the TS was immunostained with calretinin antibody (red) in a DAPI-stained section (blue). GFP fluorescence, calretinin immunoreactivity, and DAPI staining were all markedly reduced in the IT-injected transgenic mice. In (G)-(I), the TS of the transgenic and wt mice was injected (H and I) or not (G) with IT. Two weeks after the IT injection, the TS was immunostained with parvalbumin antibody (red), and the number of parvalbumin-positive cells in the TS was calculated (n = 5 animals; J). IT had no effect on GFP-negative, parvalbumin-immunoreactive interneurons. Scale bars, 200 μm (A-F); 50 μm (G-I). Columns and bars represent the mean ± SEM, respectively. ANOVA followed by Tukey post-hoc test showed no statistical differences (n.s.) among the 3 groups.